The International Journal of Advanced Manufacturing Technology (2024) 131:1347–1360
https://doi.org/10.1007/s00170-024-13013-z

ORIGINAL ARTICLE

Investigation on micro-milling of cemented carbide with ball nose and corner radius diamond-coated end mills

Daniel Figueiredo[1,2] · Joana Silva[3] · Tiago E.F. Silva[4] · Abílio M.P. de Jesus[3,4] · Cristina M. Fernandes[1] · J. Paulo Davim[2]

Received: 6 September 2023 / Accepted: 8 January 2024 / Published online: 7 February 2024

Abstract
Micro-milling of cemented carbides is a challenging task due to their high hardness, low toughness and high wear resistance. Ensuring good surface quality and dimensional accuracy is crucial for extending parts service life, which in turn enhances economical and environmental sustainability. This paper is mainly focused on evaluating surface formation mechanisms, scale effects, fracture behaviour and chip formation using distinct cemented carbide micro-milling tools with multi-layer diamond HF-CVD. In order to achieve higher precision and more efficient micro-milling operations on WC-15Co and WC-10Co, a systematic experimental approach has been carried out. The influence of cutting parameters, achievable surface quality and defects occurrence were thoroughly examined. Experimental results evidence the influence of operational conditions on the chip formation of cemented carbides as well as an important impact of the utilized cutting tool. Micro-pits, cracks, thin ploughing layer and fractured workpiece edges are amongst the observed surface damage mechanisms. A ductile cutting regime of the high-hardness composite material is confirmed, exhibited by the plastic deformation even when small depths of cut are considered.

Keywords Micro-milling · Diamond-coated carbide tools · Size effect · Surface quality · Hard materials · Cemented carbide

1 Introduction

The micro-milling of brittle hard materials in a ductile cutting mode offers a potentially valuable real-world industrial application. It enables intricate 3D features production with excellent finishing and tight tolerances, applicable to the manufacture of advanced tooling components such as powder compaction tools, microinjection moulds and dies. In addition, high-accuracy complex shape micro and miniature components made from a range of engineering materials keep pushing the market need in two main directions: the downscaling of manufacturing processes that have an existing background as conventional ones and are already widely used in industry and the development of new ones that are suitable only for this kind of manufacturing [1]. Still, the cutting phenomena at a small scale differ significantly from those observed at the macroscopic level. Size effects tend to occur once the scale of material removal, for instance the uncut chip thickness, t, or even the grain size, are comparable to the dimension of the cutting edge radius. When these length scales become comparable, several key aspects play a pivotal role in the machining behaviour. Due to the larger ratio of area to volume, tool-chip surface forces (adhesion and friction) become more significant, resulting in different cutting load scenarios thus affecting tool wear, surface finish and chip formation. The critical uncut chip thickness, t_c, is considered a key parameter in the attainment of brittle-fracture-free cutting [2–7]. This is especially relevant in cemented carbide workpieces given the minimized occurrence of surface defects (i.e., chipping and cracks) while allowing for micro-milling of complex geometries that otherwise would require relatively more time-consuming manufacturing processes, such as powder metallurgy, electrical discharge machining

✉ Daniel Figueiredo
daniel.af@ua.pt

1 R&D Department, Palbit S.A., Rua das Tilias, Branca 3850-582, Aveiro, Portugal

2 Department of Mechanical Engineering, University of Aveiro, Campus Santiago, Aveiro 3810-193, Portugal

3 DEMec, Facutly of Engineering, University of Porto, Rua Dr. Roberto Frias s/n, Porto 4200-465, Portugal

4 INEGI, University of Porto, Rua Dr. Roberto Frias 400, Porto 4200-465, Portugal

or even manual operations. Even though they can be noticed in both macro- and micro-milling [8], the size effects become more challenging to control in the latter case [9], promoting more significant defects (i.e., surface ploughing, excessive springback elastic recovery and thermal effect) when removing material at the scale of micron. According to Balazs et al. [10], size effects do not correlate linearly with tool size reduction. Even though there may be a linear relationship between t_c and the tool cutting edge radius, the workpiece grain size is also highly relevant, as stated by Li et al. [11]. For t in the same order of magnitude of grain size, chip formation might occur within a few or only a single grain of the material. Because of this, the workpiece material may not exhibit a homogenous response, which is reflected on the cutting forces and the surface quality [2, 8]. In contrast with conventional milling processes, where material can be considered to be homogeneous and isotropic, in the micro-milling process, the workpiece material must be seen as heterogeneous and, in some cases, anisotropic. As the tool moves from one metallurgical phase to another, it is expected that the cutting process will behave differently. These changes manifest themselves as load variations in the process that may lead to higher levels of vibration and pronounced tool wear/breakage. Vogler et al. [12] support such dependency by using a mechanistic model for the micro-milling process that explicitly accounts for the different phases while machining heterogeneous materials, capable of capturing higher cutting load frequencies than those that can be explained by the cutting process kinematics. Wojciechowski et al. [13] present a numerical-analytical model considering the chip thickness variation within current tool rotation (full immersion micro-end milling process of AISI 1045 steel), enabling the determination of a threshold relation for the transition from burnishing-dominant to chip formation-dominant regime (t_c/f_z=0.66). Komatsu et al. [14] studied the influence of grain size on cutting force and specific cutting energy concluding that smaller grain sizes result in a larger cutting force and specific cutting energy. This conclusion was also reached by Lauro et al. [15]. In micro-milling, the magnitude of the cutting forces is smaller compared with the conventional milling, due to the size reduction. However, the ratio of cutting force, F_c, to the passive force, F_p, differs significantly, whereby the passive force has a more significant effect on the chip removal process in micro-milling. Due to the higher influence of passive force, the ploughing effect increases and becomes more dominant than shearing responsible for chip formation. During micro-machining of hard and brittle material like cemented carbide and ceramics, the critical uncut chip thickness, t_c, can be estimated using the empirical formulas proposed by [16–18], in order to avoid unwanted scale effects and non-cutting behaviours, such as pulling of hard particles and tearing of soft phase, commonly observed in micro-milling [19, 20].

As suggested by Astakhov [21], much of our knowledge and theoretical work on conventional machining cannot be directly applied to the macro-machining of hard materials. In the field of micro-machining, the larger knowledge gap evidences the need for further studies on such materials. Subbiah and Melkote [22] summarize the size effect into two factors: ploughing forces from cutting tool edge non-zero edge radius and the increase in shear flow stress due to reduced uncut chip thickness. The authors highlight similarities between fracture-free deformation in brittle materials during machining and phenomena observed in wear/scratch tests and indentations, drawing parallels despite the distinctions in the processes. According to Davim and Jackson [23], brittle materials are difficult to process due to their hardness and crystalline nature. Material removal in the case of brittle materials depends upon the crystallographic orientation which is responsible for variation of surface finish as well as cutting forces. However, at a small depth of cuts, brittle materials behave like ductile materials. The depth of cut at which material removal is ductile is called the critical depth of cut, and the process is called ductile-regime machining. Depth of cut more than critical value leads to subsurface damage, and brittle to ductile transition also depends upon material properties and cutting forces Despite the limited data, Chen et al. [17] have studied the micro-milling of soft-brittle crystals, showing a predominance of ploughing effects when compared to shearing effect for feeds per tooth smaller than the cutting edge radius, r_β. This may result in poor surface quality due to the higher machined surface roughness. The authors also state the existence of higher specific cutting forces for smaller values of feed per tooth due to the ploughing effect, mainly for micro-end mills with a blunt cutting edge radius. Therefore, it is crucial to find out a good compromise between feed per tooth and tool stiffness, thus providing a shearing action of the cutting edge over ploughing, ensuring a good surface quality. By performing orthogonal cutting experiments on WC-11.8Co and WC-17.5Co, Ottersbach et al. [24] report differences in chip formation mechanisms due to cobalt content, having identified a maximum chip thickness of 18 μm, with a decreasing tendency for lower Co content. The minimum uncut chip thickness for both materials was found in the range of 4 to 6 μm and correlates well with the r_β/t_c of 0.3, which is characteristic of different other brittle materials such as hardened alloys and steels. Wu et al. [25] machined WC-15Co with a polycrystalline diamond (PCD) micro-end mill and they revealed that the t_c, of this material is 1.49 μm for the tested cutting conditions. Brittle cracks and micro-pits emerged (the latter due to the pull out of broken WC grains) during brittle cutting mode. These phenomena are the main causes of poor surface quality and high surface roughness. Chen et al. [17] performed experiments of micro-milling in a potassium dihydrogen phosphate crystal, which is a brittle material, reporting the existence

of micro-cracks and micro-pits in the brittle cutting mode. These last authors state that for a ratio f_z/r_β larger than 1, cracks and brittle areas start occurring in the machined surfaces, with total brittle cutting mode from f_z/r_β=3. On the other hand, $0.7< f_z/r_\beta <1$ correspond to ductile cutting conditions. Bian et al. [18] demonstrated the defects on the machined surface of ZrO_2 ceramic that originated in a brittle cutting mode. The defects were mainly micro-pits and micro-cracks, which increasingly occurred with tool wear evolution. Huo et al. [19] reported a partial ductile cutting mode when machining single-crystal silicon using a CBN micro-end mill and a diamond-coated WC micro-end mill. The partial cutting mode was considered to exist only when a few surface defects such as irregular streaks and micro-pits were left on the machined surface. When micro-pits dominated the entire surface, the authors considered that brittle cutting mode was the main mechanism. The partial ductile cutting mode is related for other authors as a transition zone between the ductile cutting mode and the brittle cutting mode. Another example of such is the work conducted by Choong et al. [20] that addressed this transition zone and explained it by the occurrence of partial brittle fracture. All mentioned authors relate cutting mode with feed per tooth. The ductile cutting mode is verified for lower values of feed per tooth and depth of cut. Cutting tools' definition presents as a significant impact on the control of the cutting regime. Wu et al. [25] have attained ductile cutting direct micro-milling of cemented carbide (WC-15Co) using a PCD micro-end mill with a large tool tip radius (prepared by wire electrical discharge machining). Using identical tool material, Yuan et al. [26] investigate the influence of tool structural design on the surface morphology and roughness of cemented carbide workpiece. The authors claim that micro-ball end mills with single-edged and spherical flank faces can avoid the phenomenon of chip blocking and depositing. Okada et al. [29] studied the cutting mechanisms of ultrasmall feed rates using diamond-coated carbide end mills on tungsten carbide workpieces. The authors report the negative impact of feed rates higher than the cross-sectional thickness of the coating film and the importance of keeping feed rates below such values for maximizing tool life. Focusing on the surface quality of cemented carbide, Okada et al. [30] have compared direct cutting using diamond-coated carbide end mill with two different common processing routes of cemented carbide: mechanical polishing and electric discharge machining (EDM). Despite having found that an identical mirror-like finish to mechanical polishing can be obtained via direct cutting, finished surfaces resulting from direct cutting were comparatively rougher than those resulting from mechanical polishing (and rougher than EDM). The authors have identified two types of surfaces: (i) flat portions of the tungsten carbide grains generated by the ductile mode cutting and (ii) uneven portions composed of fine grains generated by the brittle mode cutting. Moreover, a surface morphology with a uniform distribution of tungsten particles is noticed especially in the case of large feed rates and depth of cut conditions.

Micro-milling scale of cemented carbide shares similarities with the grinding process, where behavioural regimes have also been described. Klocke et al. [27] presented the transition from predominantly ductile to predominantly brittle material, proving that the phase fractions of the cemented carbides have a significant impact on the material behaviour. Plastic deformation can occur in the WC grains, as reported by Hegeman et al. [28], during grinding plasticity which occurs mostly in the Co, but also, there are plasticity phenomena at WC grains on the removed material.

The surface formation mechanisms, scale effects, fracture behaviour and chip formation using distinct cemented carbide during micro-milling tools with multi-layer diamond HF-CVD had not been fully described in previous studies. In this paper, the influence of HF-CVD diamond-coated cemented carbide end mills geometry is inspected on the micro-milling of cemented carbide. The influence of cobalt content and the operational parameters of the process are additionally studied. The micro-milled surface formation, chip geometry and damage mechanisms are analyzed via scanning electron microscopy in order to infer on the mechanics of micro-milling, particularly on the occurrence of ductile chip formation.

2 Experimental setup

2.1 Cutting tools, workpiece and process parameters

The cutting tools were composed of a WC-5Co substrate with a WC average grain size of 1.5 μm and 1780 HV10 hardness, fully manufactured by Palbit S.A. Their coating was achieved through the hot-filament chemical vapor deposition (HF-CVD) method, using both nano- and microcrystalline diamond layers, hereinafter referred to respectively as NCD and MCD, as depicted in Fig. 1, where the respective approximate thickness of each layer is illustrated. The coating design consists of a nucleation layer of NCD, followed by a transition layer with increasing crystalline size, culminating in the MCD layer located in the middle section of the coating. Above the MCD layer, the grain size gradient is reversed, with crystalline size diminishing progressively until the top NCD layer, completing a total of 16 μm of coating average thickness.

Two distinct tool geometries were employed in this study: (i) a micro-bull nose end mill with a tip radius of 0.1 mm, herein referred to as "bull nose", and (ii) a two-flute micro-ball end mill, herein referred to as "ball nose", with a 0.5mm tool radius (refer to Fig. 2b and d), both with a 1mm diameter.

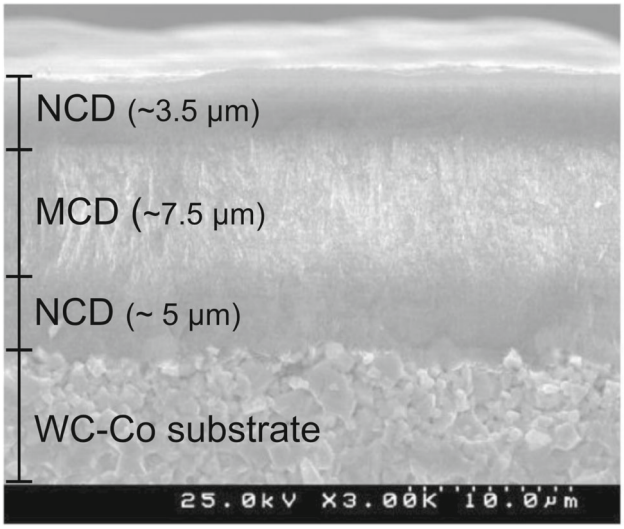

Fig. 1 Diamond coating definition of the HF-CVD micro-tools used in the study showing crystallite size distinction by layer on the tungsten carbide substrate

Their geometry is described in Table 1. A small length-to-diameter ratio was designed in order to minimize tool deflection in the micro-milling process. The distinct corner radius of each tool results in a cutting edge length of 0.5 mm for the ball nose end mill and 1.2 mm for the bull nose end mill. The rake angle and flank angle were 0°. The inclination angle of the bottom edge was 0°. The bottom and side first relief angle was 6°, which was designed to reduce the contact area between the tool bottom surface and machined surface. The cutting edge radius was measured posteriorly to cutting tool production (8 μm).

The diamond-coated micro-end mills were tested in the machining of distinct cemented carbide workpieces composed by WC-15 wt.% Co and WC-10 wt.% Co, both with 3 μm WC grain size, hardness of 1160 $\pm$ 40 HV10 and 1385 $\pm$ 40 HV10, respectively. The grades used in the experiments have 0.7% of γ-phase composed by metallic carbides, namely TiC, TaC and NbC, which are thermal stabilizers and grain growth inhibitors (this phase arises in the cemented carbide sintering stage).

A CNC milling machine (Makino IQ500) with air cooling was used for conducting the milling experiments. The cutting parameters, f_z, v_c and n, are defined as constant. Only the a_p and the a_e took different values depending on the test, as listed in Table 2. The different milling depth and feed per tooth levels were selected in order to confirm and identify the distinct chip removal conditions of cemented carbide during micro-milling. The spindle rotating speed was fixed at 45,000 rpm, corresponding to a cutting speed of 141 m/min at maximum end mill diameter. Additionally, important to note is the surface preparation process prior to the micro-milling experimental campaign (refer to Fig. 3). The sequence of machining operations and the appropriateness of the previous machined surface are decisive in attaining high-dimensional accuracy and, thus, the functionality of the micro-milled parts. All samples were submitted to a first micro-roughing stage in order to ensure the flatness of the surface and parallelism reference. A second preparation operation (micro-finishing) is conducted to improve surface quality and ensure consistency of the experimental campaign. Lubricant oil was used in the preparation stages in order to achieve an optimal surface baseline for all remaining experiments. A cemented carbide workpiece (cube) with 20 $\times$ 20 $\times$ 15 mm has been

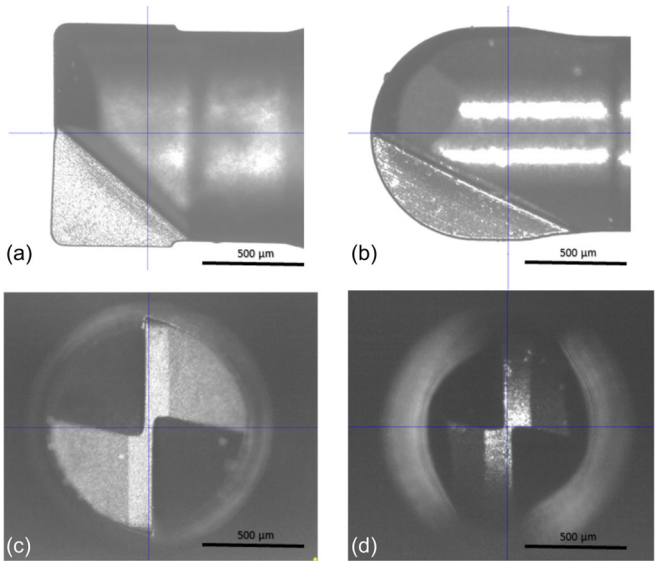

Fig. 2 Micro-end mills used in the present study: **a**) rake surface of bull nose end mill, **b**) rake surface of ball nose end mill, **c**) flank surface of bull nose end mill and **d**) flank surface of ball nose end mill

Table 1 Geometrical parameters of each end mill

Geometrical parameters	Bull nose	Ball nose
End mill diameter, D	1 mm	1 mm
Number of flutes, Z	2	2
Length of cut, l_c	1.2 mm	2.0 mm
Rake angle, γ_r	0°	0°
Flank angle, α_f	0°	0°
Cutting edge radius, $_\beta$	8 μm	8 μm

employed for the whole (surface preparation and experimental) campaign clamped to the CNC machine through a modular EROWA ITS system. The experimental campaign was performed under dry cutting conditions allowing for chip collection. Prior to the experimental texts, a surface preparation stage was performed (refer to Fig. 3f) which was the same for all the tested parameter configurations of Table 2. The cutting parameters of each surface preparation stage are described in Fig. 3a and b. Figure 3c shows the location for roughness measurements of each test (three regions of the micro-milling path were analyzed) as well as the methodology for roughness measurements (Fig. 3d) and an example of one analyzed location of a micro-milled tested region (Fig. 3e). During the test campaign, the cutting tests were always repeated once to ensure the repeatability of the controlled variables.

2.2 Setup and measurement equipment

The observation of the machined surface is crucial to identify characteristic defects that can be associated with the brittle cutting mode. The chips formed during the cutting process also indicate the cutting mode, so their observation is also essential. The morphology and the roughness of the machined surfaces and edge radius were measured with the Bruker Alicona InfiniteFocusSL, a non-contact 3D measurement system, based on focus variation. Moreover, scanning electron microscopy (SEM) was also employed to observe defect occurrence in the machined surface and chips formed during cutting tests. The resulting chip morphology (i.e., size and shape) can provide valuable information about the cutting mode and surface quality according to the operational conditions (by varying cutting parameters and milling tool definition) enabling an identification of the most appropriate cutting scenario. With regard to the machining operation, a copy (micro) milling strategy has been employed (refer to Fig. 4a) with movement in both x and y directions, including up- and down-milling. The engagement condition of each cutting tool is described in Fig. 4b and c, respectively, illustrating chip thickness according to end mill radius. Maximum thickness ($h_{\max}$) as a function of feed per tooth has been calculated, corresponding to 0.41 f_z for the ball nose and 0.91 f_z for the bull nose end mills. Despite the much smaller $h_{\max}$ promoted by the usage of the ball mill, it offers improved radial contact with the workpiece, leading to increased stability during cutting, particularly in the current scenario of shallow axial depths. Alternatively, despite its smaller radial contact with the workpiece, the bull nose may constitute an adequate cutting solution given its larger cutting diameter, combining productivity with cutting stability, which is highly required given the workpiece brittleness.

Table 2 Tested levels for each cutting parameter and for each cutting tool geometry

Cutting parameter	Levels
Spindle speed, n (rpm)	45,000
Feed per tooth, f_z(mm/z)	0.004
Radial depth of cut, $a_e(\mu$m)	5, 10
Axial depth of cut, $a_p(\mu$m)	1, 2, 4, 6, 8, 10, 20, 40, 60

3 Results and analysis

3.1 Chip formation and their size

Chip formation consistently occurred regardless of cutting conditions and WC-Co grade, for both bull nose and ball nose end mills. The chip-free surface (opposite to the side that contacts with the tool rake surface) shows striation marks due to the intense compressive and shear stresses, whereas its back surface (the side of the chip that contacts with the tool rake face) is smoother, as shown in Fig. 5. This smooth chip back surface aspect is a good indicator of the presence of the ductile cutting mode, promoted by tool-chip sliding with low friction conditions, as concluded by Bian et al. [18] and Antwi et al. [31]. On the cutting test with the bull nose end mill, there seems to be a difference in the chip formation behaviour, especially in conditions of lower average chip thickness. Still, the brittle cutting mode does not seem to completely dominate the chip formation mechanism; otherwise, only long material particles could be seen, and no chips could be perfectly detached, as referred by Liu et al. [32]. As shown in Fig. 5 and further supported by Figs. 6, 7 and 8, the critical uncut chip thickness, t_c, was achieved for a portion of the full chip length in both micro-mills. This means that due to the variable thickness of the obtained chips, a portion of its length is under the t_c ductile threshold, whereas another portion is above it, explaining the very significant differences in the size of chips and fragments, illustrated in Fig. 5.

Figures 6 and 7 show a representative impact of WC-15Co and WC-10Co collected chips for each tested condition of micro-milling, using the same cutting tool (ball nose). For

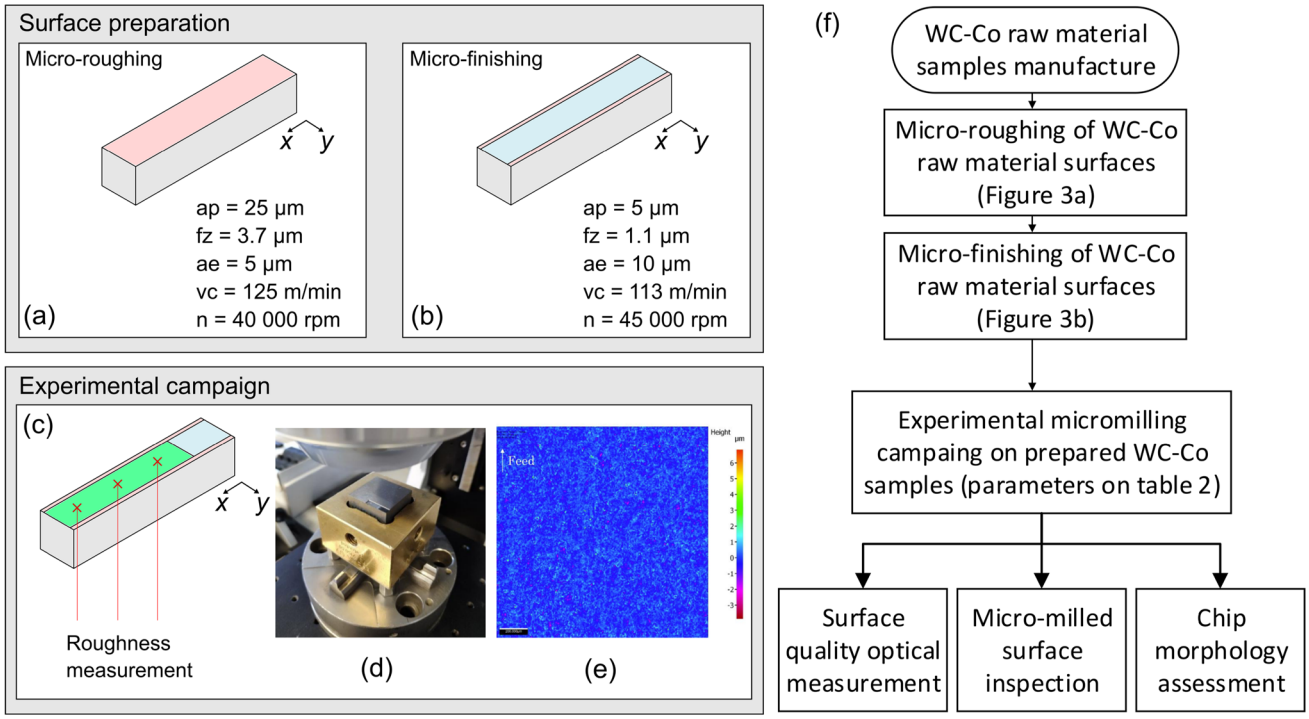

Fig. 3 Stages of surface preparation and experimental campaign: **a**) micro-roughing first surface preparation stage, **b**) micro-finishing second surface preparation stage, **c**) experimental campaign and surface measurement location at each micro-milled slot, **d**) surface roughness analysis setup, **e**) surface roughness results and **f**) flowchart of the experimental work and analysis

both tested material grades and operative conditions (a_e and a_p), small chip fragments can be observed, more evidently on the carbide grade with the lower amount of Co binder. The fragments can also be resultant from chips that get into the tool path (interference, as dry cutting process zone), during the micro-milling process. From Figs. 6 and 7, it is additionally possible to observe that the needle-shaped chips formed with the two-flute ball nose end mill have a flat rather than curled appearance for both WC-Co grades.

From the analysis and direct comparison of Figs. 6 and 8, it is possible to confirm the considerable impact of the cutting edge configuration presented in Fig. 4. The ball nose micro-end mill edges (with a bigger radius) allow a cutting process with larger plastic deformation and longer chips; the same does not seem valid for the smaller radius tool (bull nose), despite its larger average uncut chip thickness.

Figure 9 shows the relation between chip average size in function of operative conditions for both WC-15Co and WC-

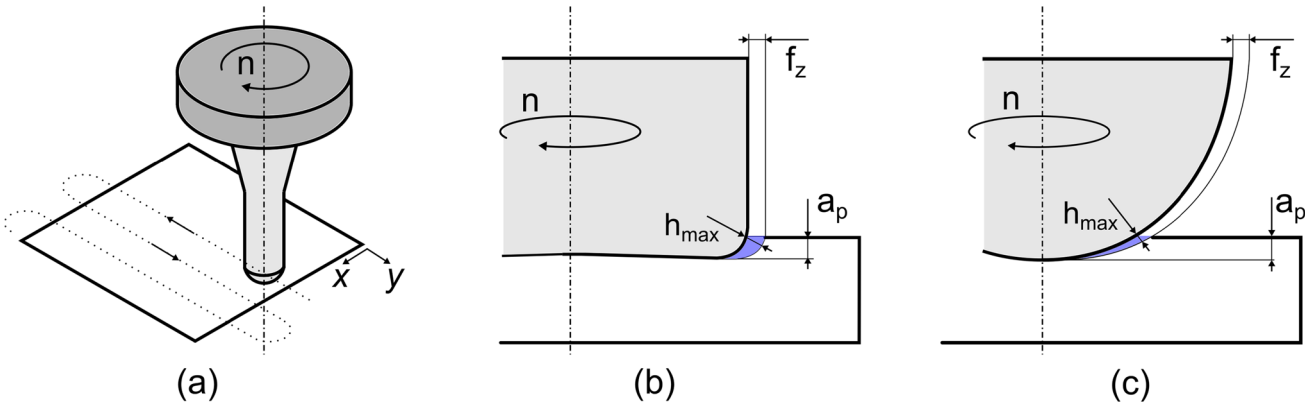

Fig. 4 Scheme of the employed surface copy milling strategy, including up- and down (micro) milling (**a**); micro-milling maximum chip thickness (h_{max}) illustration for bull (**b**) and ball (**c**) nose end mills, under the specified operational cutting conditions

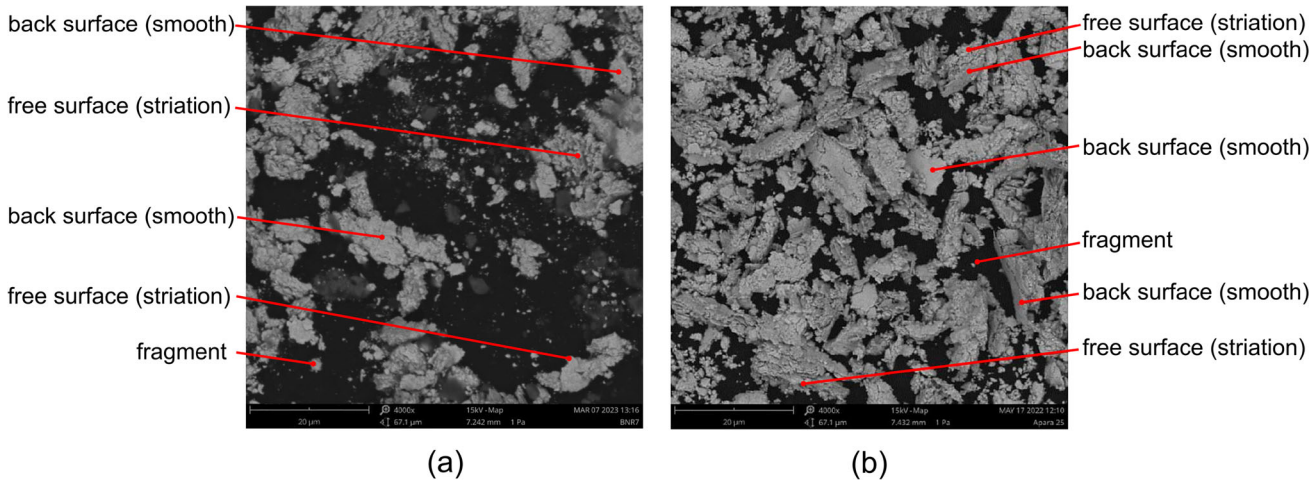

Fig. 5 Characterization of the WC-Co chips formed with: **a**) two-flute micro-bull nose and **b**) micro-ball end mill using $a_p = 4\ \mu$m and $a_e = 5\ \mu$m

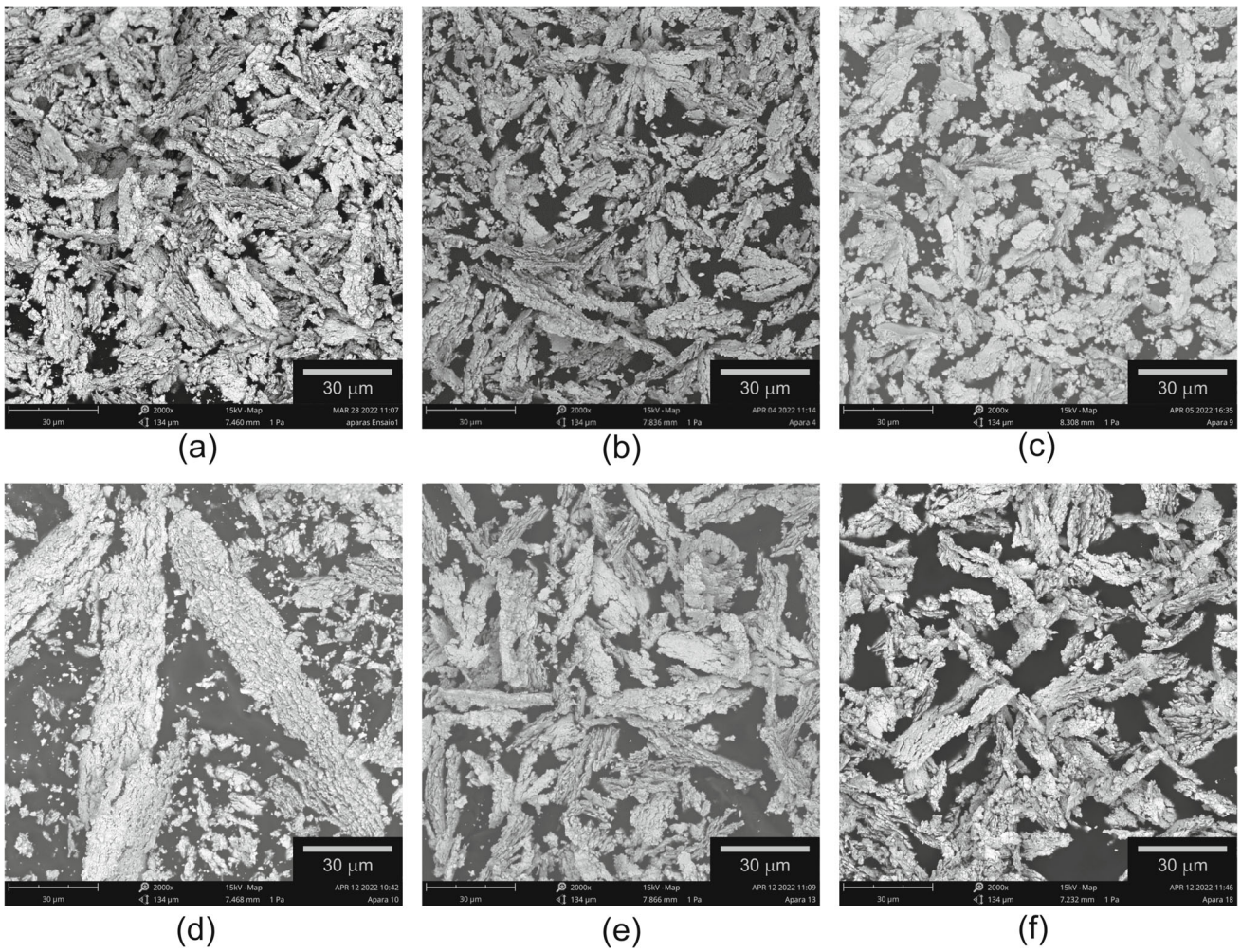

Fig. 6 SEM images showing the resultant chip morphology from WC-15Co workpiece using a ball nose end mill under the cutting conditions: **a**) a_p=60 μm, a_e=5 μm; **b**) a_p=10 μm, a_e=5 μm; **c**) a_p=1 μm, a_e=5 μm; **d**) a_p=60 μm, a_e=10 μm; **e**) a_p=10 μm, a_e=10 μm; **f**) a_p=1 μm, a_e=10 μm

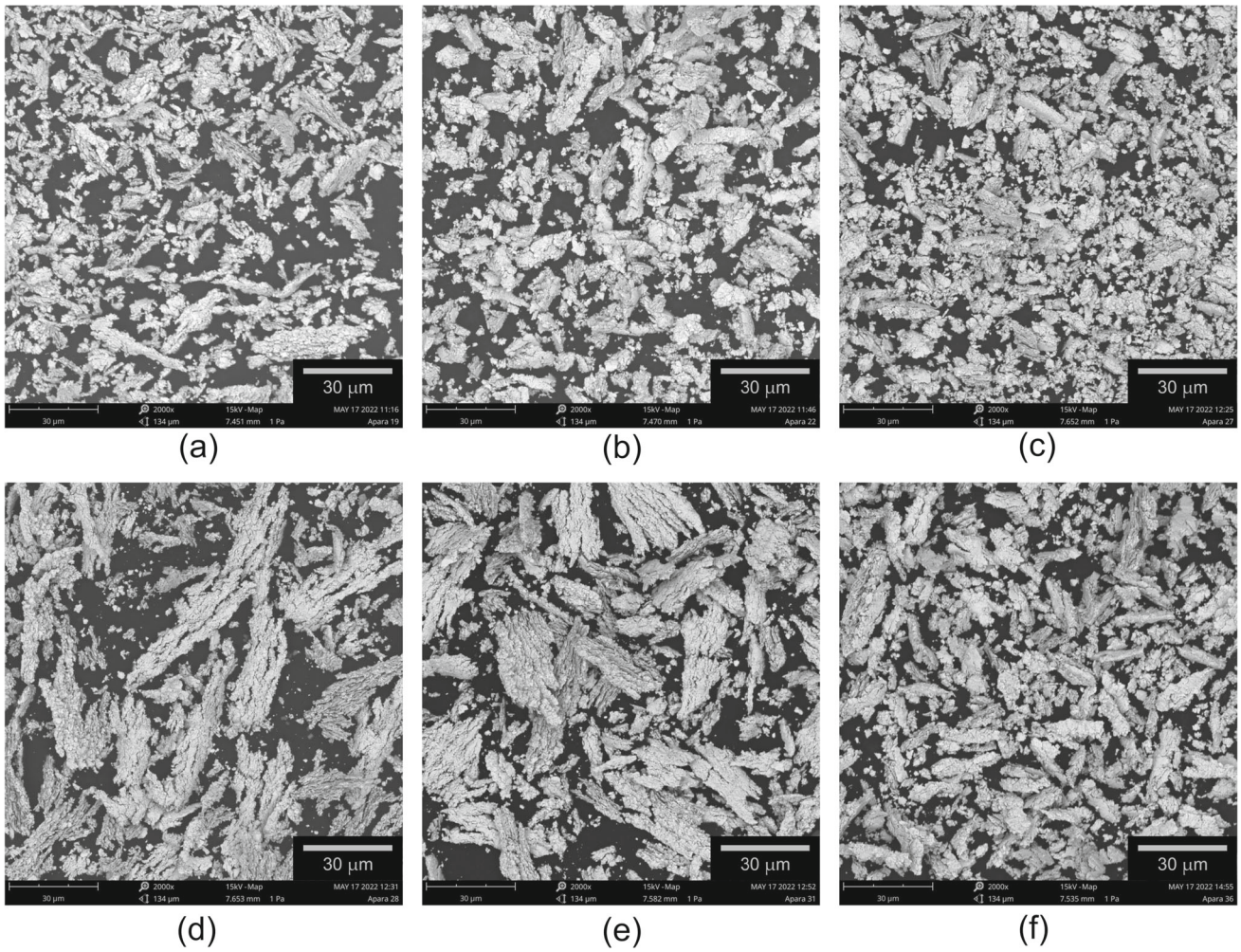

Fig. 7 SEM images showing the resultant chip morphology from WC-10Co workpiece using a ball nose end mill under the cutting conditions: **a**) a_p=60 μm, a_e=5 μm; **b**) a_p=10 μm, a_e=5 μm; **c**) a_p=1 μm, a_e=5 μm; **d**) a_p=60 μm, a_e=10 μm; **e**) a_p=10 μm, a_e=10 μm; **f**) a_p=1 μm, a_e=10 μm

10Co materials. Despite some scatter (potentially resultant from chip fragmentation degree), it is verified that chip size increases with axial depth of cut, which reinforces the idea inferred by Figs. 6, 7 and 8. Even though a representative sample of chips was selected (larger than 100 samples digitally measured), the average chip size will certainly be influenced by the fragmentation phenomenon. Also, interesting to note is that the linear fit to the experimental data tends to a non-zero chip size for very small axial depths of cut, evidencing the existence of a minimum chip size L_{ch} which, depending on the operational conditions, may amount to 8 to 18 μm, approximately. While the ductile-to-fragile transition is readily discernible in various materials, it remains less clearly defined within this particular composite material. The geometry condition of the cutting edge is not directly represented in the critical depth model of the equation presented by Bifano et al. [33] nor detailed on micro-milling evaluations of Neo et al. [34] and Cheng et al. [35].

While the bull nose and ball nose chips generated during micro-milling exhibit distinct visual differences at a macroscopic level (refer to Fig. 5), a closer examination at high magnification (refer to Fig. 10) reveals a remarkable equivalence between the two. Despite their macro-apparent variation in shape, both chip types retain the elements of the removed material, namely tungsten carbide (WC) and cobalt (Co). This can be confirmed by the EDS analysis conducted for each type of chip (refer to Fig. 10). Such observation emphasizes the underlying consistency in the material removal process and highlights the presence of those elements within the chips, suggesting identical (very large deformation) fundamental principles governing both micro-end mills on cemented carbides workpieces.

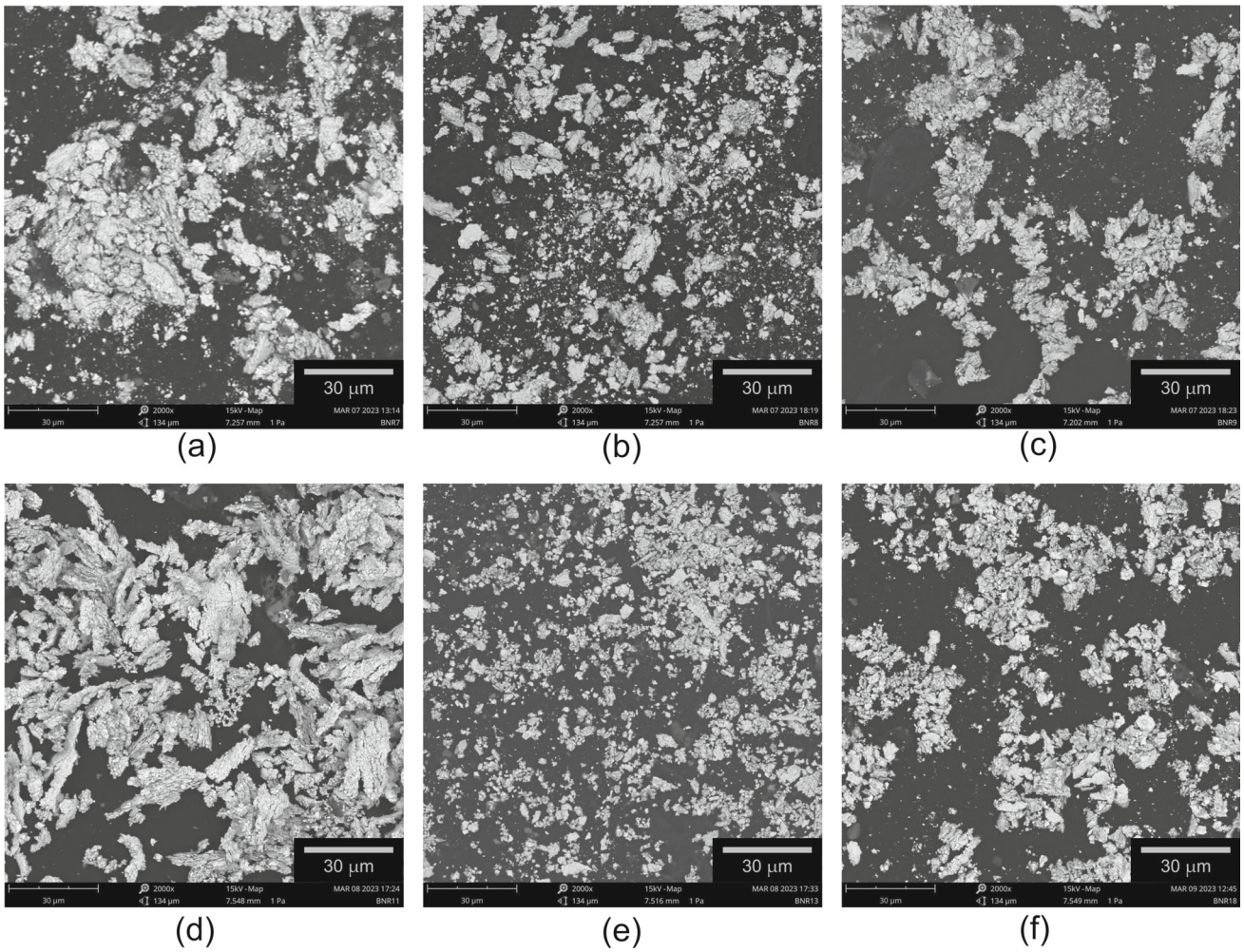

Fig. 8 SEM images showing the resultant chip morphology from WC-15Co workpiece using a bull nose end mill under the cutting conditions: **a**) a_p=60 μm, a_e=5 μm; **b**) a_p=10 μm, a_e=5 μm; **c**) a_p=1 μm, a_e=5 μm; **d**) a_p=60 μm, a_e=10 μm; **e**) a_p=10 μm, a_e=10 μm; **f**) a_p=1 μm, a_e=10 μm

3.2 Machined surface characterization

The arithmetical mean deviation (Sa) results, obtained through 3D microtopography, are shown in Fig. 11, enabling surface quality assessment and control. Those results show that surface quality is not sensitive to the axial depth of cut, regardless of the tested operative conditions or %Co of the workpiece. This observation is consistent with the idea that the minimum chip thickness was reached within stable chip formation, thus resulting in the possible lowest roughness values regardless of remaining process variables. Alternatively, the relatively improved surface quality of the ball nose end mill over the bull nose is evidenced, supporting the significant influence of the tool edge definition, in particular the extent of radial contact with the workpiece. The more uniform engagement of the ball nose end mill seems to result in enhanced cutting stability, avoiding tool chatter which

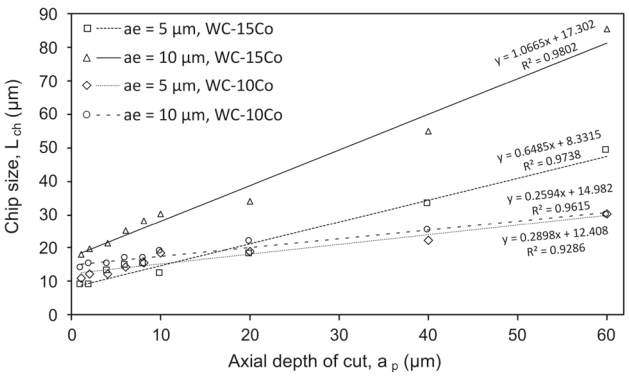

Fig. 9 Influence of axial depth of cut, a_p, and radial depth of cut, a_e, on the chip size evolution using a ball nose end mill on 15% and 10% cobalt content tungsten carbide

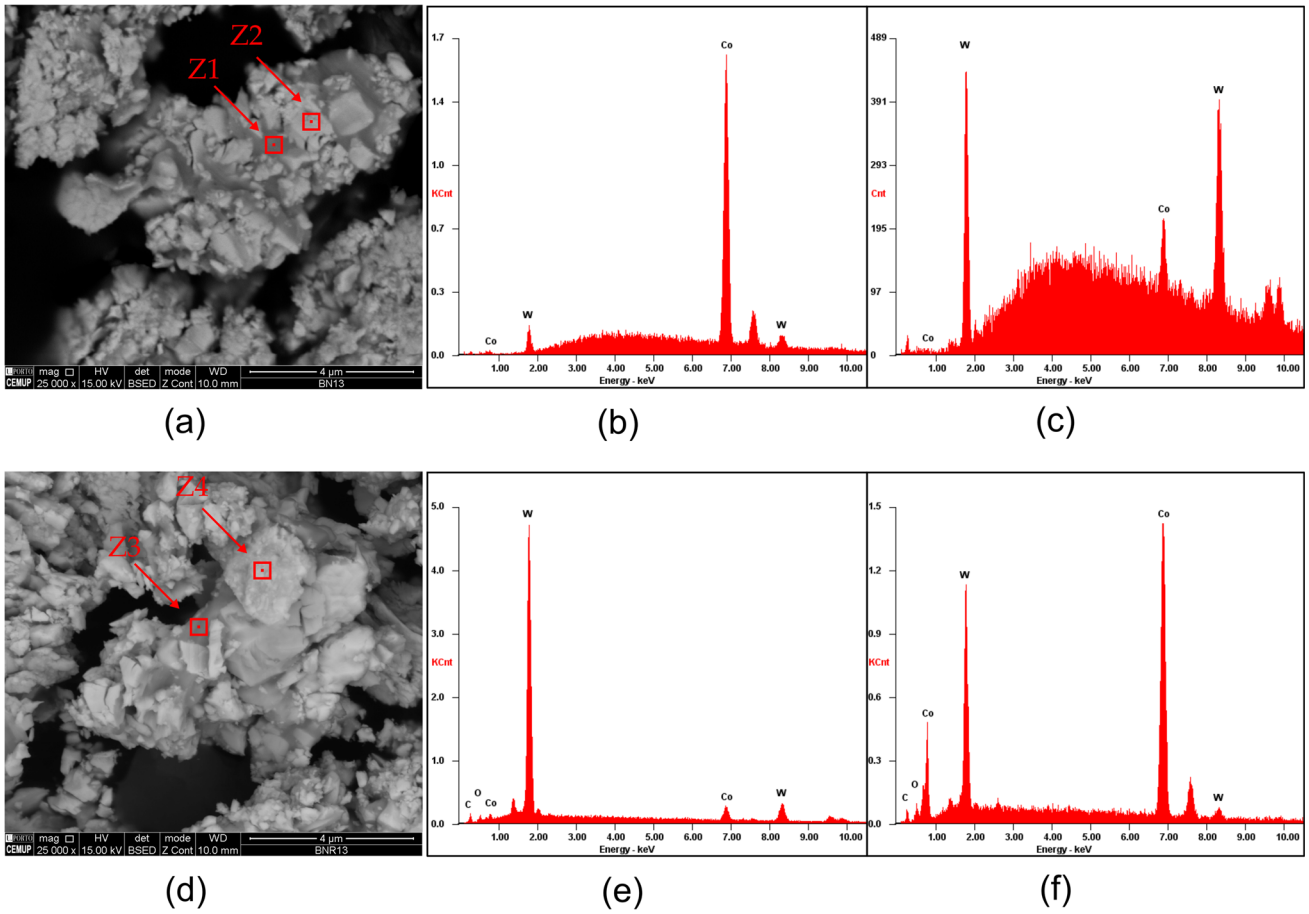

Fig. 10 EDS analysis and morphology of selected chips from ball nose end mills (**a**), EDS-points analysis Z1 (**b**), EDS-points analysis Z2 (**c**), chips from bull nose end mills (**d**)), EDS-points analysis Z4 (**e**) and EDS-points analysis Z3 (**f**), using an a_p of 10 μm, f_z of 4 μm/z and a_e of 10 μm on the 15% Co tungsten carbide workpiece, evidencing the existence of both WC and Co regardless of chip morphology

could lead to surface imperfections. In sum, the geometrical influence of the tool seems to surpass any variation to the cutting phenomenon imposed by the distinct tested operational conditions.

Figure 12 depicts the resultant machined surface and defect occurrence in the micro-milling experiments. In particular, Fig. 12a shows the transition between the original (non-milled) and micro-milled surface, using the two-flute ball nose micro-milling cutter. Whereas in the non-milled surface, WC grains in a cobalt matrix can be observed, in the micro-milled surface, the WC grains are indiscernible, suggesting their intensive deformation and fracture. A larger micro-milled area can be seen in Fig. 12b, where surface defects (such as micro-pit occurrence and cracking can be noticed). Notability, tool engagement can lead to significant degradation of the workpiece edges. This emphasizes the necessity for precise control of the micro-milling strategies near the workpiece edges. An alternative to the proposed machining strategy could be a peripheral finishing stage after the surface end machining. Figure 12c provides a closer examination of edge degradation. The presence of cracked WC grains, coupled with the absence of visible morphological changes, strongly indicates the occurrence of brittle fracture along the edges of the micro-milled samples. These defects pose a challenge as there is a risk of their propagating within the edge region, extending to the generated micro-milled surface which may potentially compromise the

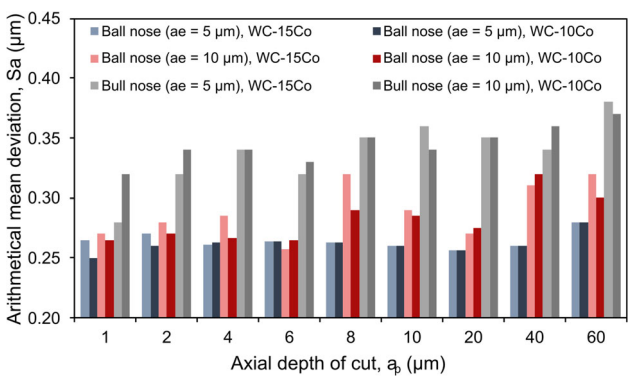

Fig. 11 Arithmetic mean deviation (Sa) obtained from the performed experimental campaign

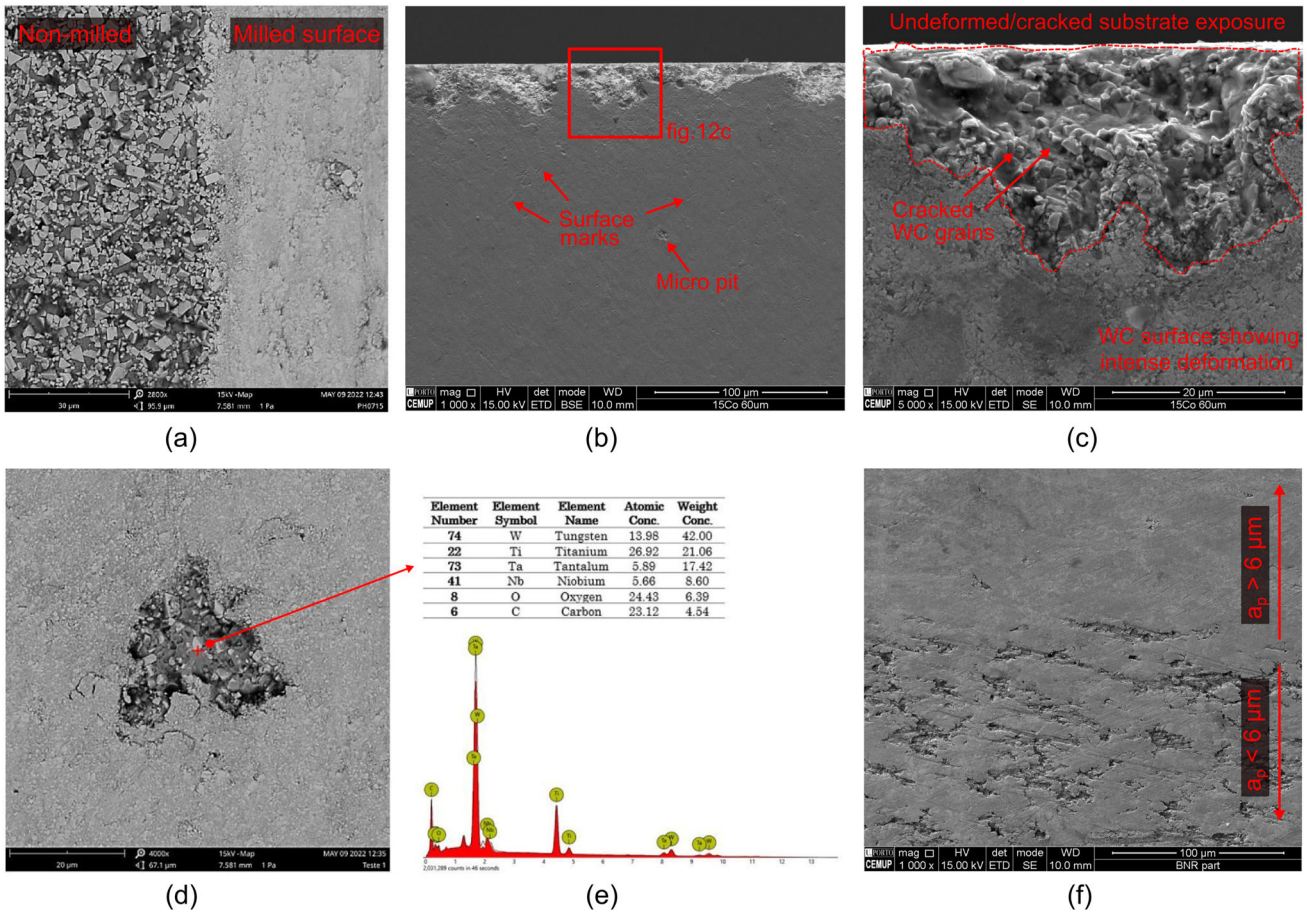

Fig. 12 Micro-milled surface observation under scanning electron microscopy: **a**) original (non-milled) and milled surfaces, evidencing the intense deformation of the WC grains; **b**) micro-pit and edge deterioration defects; **c**) surface crack defects at workpiece edge surface; **d**) micro-pit defect submitted to **e**) EDS analysis; **f**) effect of depth of cut on surface processing appearance

functionality of added-value components. In some observed micro-pits, detailed in Fig. 12d and e, energy-dispersive X-ray spectroscopy (EDS) analysis revealed the presence of Ti, Ta and Nb-characteristic elements of the WC-Co γ-phase, rich in TiC/TaC and NbC. This γ-phase does not undergo plastic deformation due to its high hardness, leading to its removal from the machined surface. Micro-pit occurrence was verified in almost all experiments, in both WC-15Co and WC-10Co materials.

Depending on operational cutting conditions, traces/marks on milled surfaces were observed, as illustrated in Fig. 12b. These traces may result from either the cutting test or surface preparation. Due to limited material removal during micro-milling tests, especially for smaller a_p, there may be instances where residual marks from preceding tools, along with surface imperfections like micro-pits, cannot be entirely removed.

Figure 12f confirms that below $a_p \leq 6$ μm, the generated ploughing layer does not completely cover the machined surface. This indicates a reduction in ductile deformation on the material, with increasingly large areas of surface defects and exposed WC carbide.

In Fig. 13, the deformation phenomenon occurring in both WC-15Co and WC-10Co workpiece materials is illustrated. This analysis focuses on the affected layer beneath the machined surface, due to its exposure promoted by workpiece edge deterioration. The affected layer exhibits evidence of ploughing, a consequence of micro-machining size effects as referred to in the literature. Figure 13b and c demonstrate the presence of some cracked WC grains below the thin ploughing layer. In both tested WC-Co grades, the identification of ploughing layer limits and its thickness calculation was revealed to be a challenging task. Although this layer appears to have a thickness in the nanometre range, the SEM analysis seems to show that the ploughing layer is a combination of Co with small fragments of WC grains. This morphology of ploughing layer appears to be valid for both material grades and tested tools. Since both material grades have a grain size of 3 μm, this may indicate that machining leads to the fragmentation of WC grains during

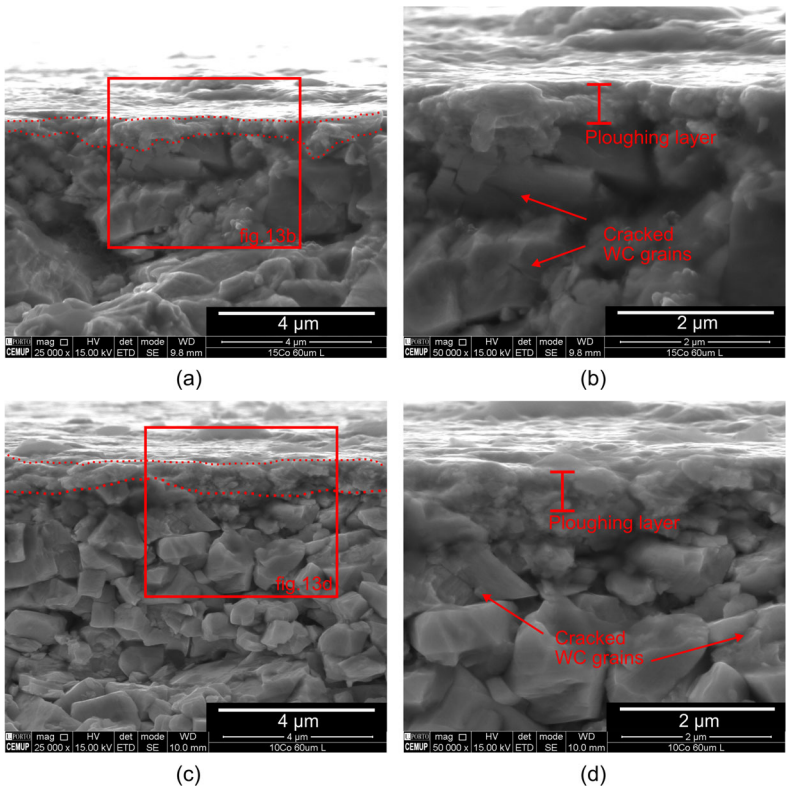

Fig. 13 SEM images of the perpendicular-to-milled surfaces for workpiece material with 15% Co (**a** and **b**) and 10% Co (**c** and **d**) tungsten carbide (a_p= 60 μm; a_e=5 μm)

chip removal or a rearrangement of the ploughing layer and substrate.

4 Conclusions

The developed work contributes to the comprehension of the intricate nature of microfabrication. The downsizing of products presents new challenges and calls for novel machining approaches. This transition benefits from the reassessment of tool technology, material behaviour and mechanical/tribological cutting conditions especially in what concerns ductile chip formation in hard brittle material workpieces. The ductile chip formation process remained consistent irrespective of cutting conditions and WC-Co grade, despite the inherent brittleness of the material. Even though the more consistent chip morphology was obtained with the ball nose micro-end mills (needle-shape), that phenomenon was observed regardless of tool geometry. Despite the predominance of ductile cutting mode, responsible for smooth surfaces, brittle cutting seems to coexist (presence of small workpiece material fragments) resulting in small surface defects. The average chip size is smaller for the WC-10Co material than for the WC-15Co material, for both tested micro-cutters. Such is related with the lower Co content of the tested material grade and, thus, its relatively higher brittleness (lower toughness).

The results of these investigations can be summarized as follows:

1. A linear increasing tendency in chip size (L_{ch}) with depth of cut corroborates the ductile chip formation mechanism. Moreover, the existence of a minimum chip size is evidenced by the fact that L_{ch} tends to a non-zero value for very small axial depths of cut. Depending on the operational conditions, the minimum chip size may amount to 8 to 18 μm, approximately.
2. Surface quality remains independent from operative conditions or workpiece %Co. This consistency aligns with minimum chip thickness occurring during stable chip formation, resulting in optimal (minimal) roughness. Moreover, the ball nose's uniform engagement seems to enhance stability, preventing tool chatter and surface defects.
3. The machined material has a high-volume fraction of binder (Co), 15% by mass but more than 23.7% by volume, having even more impact on the reported ductile deformation of the Co removed in the chips. However, as has already been reported by other researchers who have studied deformation in the grinding process, plastic

deformation of the removed WC grain was not confirmed and more research is needed to detail the ductile behaviour of these multi-phase brittle materials and contribute to a clear description of the occurring material behaviour mechanisms.

4. The ball nose micro-end mill edges (with a bigger radius) allow a cutting process with larger plastic deformation and (35%) longer chips than the ones obtained with the smaller radius tool (bull nose).
5. For operational conditions smaller than a_p=50 μm, a_e=10 μm and f_z=4 μm/z using a bull nose end mill, the deformation regime becomes quite unstable (fragmented chips increase). Still, the brittle cutting mode does not seem to completely dominate the chip formation mechanism; otherwise, only long material particles/fragments could be seen, and no chips would be perfectly detached.
6. SEM images reveal a ploughing layer (approximately 1 μm or smaller) for all ap values, for both WC-Co grades with the two-flute micro-ball end mill with sub-grain thickness, which is an evidence of the ductile cutting regime.
7. A minimum depth of cut (6 μm) has been identified, below which the generated ploughing layer does not completely cover the machined surface. This indicates a reduction in ductile deformation on the material, with increasingly large areas of surface defects and exposed WC carbide. Consequently, machining operations at depths less than 6 μm may lead to compromised surface integrity, susceptibility to wear and a decline in overall material performance.
8. From the observation and measured Sa, the surface quality is not sensitive to the axial depth of cut, regardless of the tested operative conditions or %Co of the workpiece; relatively improved surface quality (20% in average) of the ball nose end mill over the bull nose is evidenced, supporting the significant influence of the tool edge definition.
9. Micro-pit surface defects resultant from the detachment of γ-phase high-hardness cemented carbide zones from the machined surface were confirmed in both tested 10% Co and 15% Co cemented carbides.
10. The implemented micro-tool path (copy milling in two directions) can lead to noticeable degradation of the workpiece edge. Different micro-milling strategies should be implemented near the workpiece edges (i.e., peripheral finishing) for minimizing their degradation.

Author contribution DF and TEFS conceived the idea of the manuscript. JS and DF performed the experimental machining work. All authors provided critical feedback and helped shape the research, analysis and manuscript.

Funding Open access funding provided by FCT|FCCN (b-on). The authors gratefully acknowledge the funding of Project Hi-rEV - Recuperação do Setor de Componentes Automóveis (C644864375-00000002) cofinanced by Plano de Recuperação e Resiliência (PRR), República Portuguesa, through NextGeneration EU.

Declarations

Conflict of interest The authors declare no competing interests.

References

1. Rakesh PK, Davim JP (2023) Innovative development in micro-manufacturing processes. CRC Press. https://doi.org/10.1201/9781003364948
2. De Oliveira FB, Rodrigues AR, Coelho RT, De Souza AF (2015) Size effect and minimum chip thickness in micromilling. Int J Mach Tools Manuf 89, 39–54. Elsevier Ltd. https://doi.org/10.1016/j.ijmachtools.2014.11.001
3. Niu Z, Jiao F, Cheng K (2018) An innovative investigation on chip formation mechanisms in micro-milling using natural diamond and tungsten carbide tools. J Manuf Process 31, 382–394. Elsevier Ltd. https://doi.org/10.1016/j.jmapro.2017.11.023
4. Ducobu F, Filippi E, Rivière-Lorphèvre, (2009) Chip formation and minimum chip thickness in micro-milling. Proc CIRP 1:339–346
5. Sahoo P, Patra K, Szalay T, Dyakonov AA (2020) Determination of minimum uncut chip thickness and size effects in micro-milling of P-20 die steel using surface quality and process signal parameters. Int J Adv Manuf Technol 106(11-12), 4675–4691. Springer. https://doi.org/10.1007/s00170-020-04926-6
6. Yang M, Li C, Zhang Y, Jia D, Zhang X, Hou Y, Li R, Wang J (2017) Maximum undeformed equivalent chip thickness for ductile-brittle transition of zirconia ceramics under different lubrication conditions. Int J Mach Tools Manuf, 122, 55–65. Elsevier Ltd. https://doi.org/10.1016/j.ijmachtools.2017.06.003
7. Lai X, Li H, Li C, Lin Z, Ni J (2008) Modelling and analysis of micro scale milling considering size effect, micro cutter edge radius and minimum chip thickness. Int J Mach Tools Manuf 48(1):1–14. https://doi.org/10.1016/j.ijmachtools.2007.08.011
8. Chen N, Li HN, Wu J, Li Z, Li L, Liu G, He N (2021) Advances in micro milling: from tool fabrication to process outcomes. Int J Mach Tools Manuf 160. https://doi.org/10.1016/j.ijmachtools.2020.103670
9. O'Toole L, Kang CW, Fang FZ (2021) Precision micro-milling process: state of the art. Adv Manuf, 9(2), 173–205. Shanghai University. https://doi.org/10.1007/s40436-020-00323-0

10. Balázs BZ, Geier N, Takács M, Davim JP (2021) A review on micro-milling: recent advances and future trends. Int J Adv Manuf Technol 112(3–4):655–684. https://doi.org/10.1007/s00170-020-06445-w
11. Li Y, Cheng X, Ling S, Zheng G, Liu H, Wang F (2021) Study on micro cutting fundamentals considering the cutting edge radius and the workpiece material in micro end milling. Proc Inst Mech Eng, Part E: J Process Mech Eng 235(1), 93–102. SAGE Publications Ltd. https://doi.org/10.1177/0954408920946024
12. Vogler MP, DeVor RE, Kapoor SG (2003) Microstructure-level force prediction model for micro-milling of multi-phase materials. J Manuf Sci Eng 125(2):202. https://doi.org/10.1115/1.1556402
13. Wojciechowski S, Matuszak M, Powałka B, Madajewski M, Maruda RW, Królczyk GM (2019) Prediction of cutting forces during micro end milling considering chip thickness accumulation. Int J Mach Tools Manuf 147. https://doi.org/10.1016/j.ijmachtools.2019.103466
14. Komatsu T, Yoshino T, Matsumura T, Torizuka S (2012) Effect of crystal grain size in stainless steel on cutting process in micromilling. Proc CIRP 1:150–155. https://doi.org/10.1016/j.procir.2012.04.026
15. Lauro CH, Brandão LC, Carou D, Davim JP (2015) Specific cutting energy employed to study the influence of the grain size in the micro-milling of the hardened AISI H13 steel. Int J Adv Manuf Technol 81(9–12):1591–1599. https://doi.org/10.1007/s00170-015-7321-x
16. Wu X, Li L, He N, Zhao G, Shen J (2019) Investigation on the surface formation mechanism in micro milling of cemented carbide. Int J Refract Met Hard Mater 78, 61–67. Elsevier Ltd. https://doi.org/10.1016/j.ijrmhm.2018.09.001
17. Chen N, Chen M, Wu C, Pei X, Qian J, Reynaerts D (2017) Research in minimum undeformed chip thickness and size effect in micro end-milling of potassium dihydrogen phosphate crystal. Int J Mech Sci 134:387–398. https://doi.org/10.1016/j.ijmecsci.2017.10.025
18. Bian R, Ferraris E, Ynag Y, Qian J (2018) Experimental investigation on ductile mode micro-milling of ZrO2 ceramics with diamond-coated end mills. Micromachines 9(3):127. https://doi.org/10.3390/mi9030127
19. Huo D, Lin C, Choong ZJ, Pancholi K, Degenaar P (2015) Surface and subsurface characterisation in micro-milling of monocrystalline silicon. Int J Adv Manuf Technol 81(5–8):1319–1331. https://doi.org/10.1007/s00170-015-7308-7
20. Choong ZJ, Huo D, Degenaar P, O'Neill A (2019) Micromachinability and edge chipping mechanism studies on diamond micro-milling of monocrystalline silicon. J Manuf Process 38, 93–103. Elsevier Ltd. https://doi.org/10.1016/j.jmapro.2019.01.004
21. Astakhov VP (2011) Machining of hard materials - definitions and industrial applications. In: Machining of hard materials, Springer London, pp 1–32. https://doi.org/10.1007/978-1-84996-450-0
22. Subbiah S, Melkote SN (2013) Engineering materials for micro cutting. Micro-cutting: fundamentals and applications, 87–114. Wiley Online Library. https://doi.org/10.1002/9781118536605
23. Davim JP, Jackson MJ (2009). Nano and micromachining. Wiley Online Library. https://doi.org/10.1002/9780470611807
24. Ottersbach M, Zhao W (2016) Experimental investigations on the machinability of tungsten carbides in orthogonal cutting with diamond-coated tools. Proc CIRP 46:416–419. https://doi.org/10.1016/j.procir.2016.04.008
25. Wu X, Li L, He N, Zhao G, Shen J (2019) Experimental investigation on direct micro milling of cemented carbide. Micromachines, 10(2), 147. MDPI AG. https://doi.org/10.3390/mi10020147
26. Yuan H, Zhao W, Liang Z, Li S, Wang X, Zhou T, Sun X, Jiang L (2020) Structural design and fabrication of polycrystalline diamond micro ball-end mill. Int J Adv Manuf Technol, 108, 1899–1911. Springer. https://doi.org/10.1007/s00170-020-06092-6
27. Klocke F, Wirtz C, Mueller S, Mattfeld P, (2016) Analysis of the material behavior of cemented carbides (WC-Co) in grinding by single grain cutting tests. Procedia CIRP, 209(13). https://doi.org/10.1016/j.procir.2016.03.209
28. Hegeman JBJW, Hosson JThMD, With G (2001) Grinding, hardmetals, abrasive machining, roughness. Residual stress. WEAR 187–196. https://doi.org/10.1016/S0043-1648(00)00561-5
29. Okada M, Yoshida A, Furumoto T, Watanabe H, Asakawa N, Otsu M (2016) Mechanisms and characteristics of direct cutting of tungsten carbide using a diamond-coated carbide end mill. Int J Adv Manuf Technol 86(5–8):1827–1839. https://doi.org/10.1007/s00170-015-8324-3
30. Okada M, Shinya M, Kondo A, Watanabe H, Sasaki T, Miura T, Otsu M (2021) Surface quality of cemented tungsten carbide finished by direct cutting using diamond-coated carbide end mill. J Manuf Process 61:83–99. https://doi.org/10.1016/j.jmapro.2020.11.004
31. Antwi, E. K, Liu, K, Wang, H (2018). A review on ductile mode cutting of brittle materials. Frontiers Mech Eng 13(2), 251–263. Higher Education Press. https://doi.org/10.1007/s11465-018-0504-z
32. Liu K, Li XP, Rahman M, Liu XD (2004) A study of the cutting modes in the grooving of tungsten carbide. Int J Adv Manuf Technol 24(5–6):321–326. https://doi.org/10.1007/s00170-003-1565-6
33. Bifano TG, Dow TA, Scattergood RO (1991) Ductile-regime grinding: a new technology for machining brittle materials. J Eng Ind 113(2):184–189. https://doi.org/10.1115/1.2899676
34. Neo WK, Kumar AS, Rahman M (2012) A review on the current research trends in ductile regime machining. Int J Adv Manuf Technol 63(5–8):465–480. https://doi.org/10.1007/s00170-012-3949-y
35. Cheng X, Wei XT, Yang XH, Guo YB (2014) Unified criterion for brittle-ductile transition in mechanical microcutting of brittle materials. J Manuf Sci Eng 136(5). https://doi.org/10.1115/1.4027996